Journal of Aerosol Science 182 (2024) 106440

Contents lists available at ScienceDirect

Journal of Aerosol Science

journal homepage: www.elsevier.com/locate/jaerosci

Evidence of oxygenated species in laser-irradiated carbon particles

Francesca Migliorini [a], Roberto Dondé [a], Andrea Lucotti [b], Mauro Fasoli [c], Matteo Tommasini [b,**], Silvana De Iuliis [a,*]

[a] CNR-ICMATE, Istituto di Chimica della Materia Condensata e di Tecnologie per l'Energia, CNR, Milano, Italy
[b] Dipartimento di Chimica, Materiali e Ingegneria Chimica "G. Natta", Politecnico di Milano, Milano Italy
[c] Dipartimento di Scienza dei Materiali, Università di Milano-Bicocca, Milano, Italy

ARTICLE INFO

Handling Editor: Chris Hogan

Keywords:
Laser irradiation
FT-IR
Raman spectroscopy
Absorption coefficient
Carbon nanoparticles

ABSTRACT

Combustion-generated carbon nanoparticles exhibit a variety of optical and physicochemical properties. Therefore, when applying laser diagnostic tools for monitoring purpose, it is important to consider the different response of the particles with varying properties as well as the impact of laser irradiation on these properties. In this work, we analyze the possible modification of particle optical and physicochemical properties by coupling extinction measurements with FT-IR and Raman spectroscopy. The aim is to retrieve optical, chemical, and structural properties of the particles under analysis. To our knowledge, the approach proposed in this work has not yet been performed on irradiated particles. Particles are sampled from a premixed flame at two heights above the burner, representing two different aging stages. While extinction measurements are carried out in-flow, FT-IR and Raman spectroscopy are performed on particles collected for ex-situ analysis. Moreover, the analysis is conducted on both pristine and irradiated nanoparticles with one and ten laser shots. While nascent particles do not exhibit relevant modification under laser irradiation, heating mature particles with one or more laser pulses of relatively high energy density is observed to significantly affect absorption properties, particle structures and specific surface functionalities. The presence of oxygenated species in mature particles and in particular the structures spectroscopically correlated with graphene oxide indicates that specific chemical reaction pathways can occur under laser irradiation, likely promoted in the ambient condition under analysis.

1. Introduction

Carbon nanoparticles produced in combustion processes exhibit different optical and physicochemical properties depending on the specific combustion conditions (residence time, temperature, C/O ratio) and fuel employed (Michelsen et al., 2017, 2020). Specifically, nascent particles with amorphous structures and low C/H ratio present low absorption coefficient, although with a significant wavelength dependence. In contrast, mature particles exhibit higher C/H ratio with ordered/graphitic nanostructures and significantly higher absorption coefficient. The variety of these properties can produce different impact both on human health and environment. Additionally, for the implementation of diagnostic tools for monitoring purposes particular care must be taken regarding the optical properties of the particles under analysis. Different responses can be produced depending on the initial soot particle properties.

* Corresponding author.
** Corresponding author.
E-mail addresses: matteo.tommasini@polimi.it (M. Tommasini), silvana.deiuliis@cnr.it (S. De Iuliis).

https://doi.org/10.1016/j.jaerosci.2024.106440
Received 30 May 2024; Received in revised form 23 July 2024; Accepted 30 July 2024
Available online 3 August 2024

Furthermore, if laser diagnostics are employed, changes in these properties must be considered for a correct interpretation of the optical signals.

In this context, few works are reported in the literature on the analysis of the effects of laser irradiation on the properties of carbon nanoparticles, which mainly depend on the experimental conditions employed, (*e.g.*, premixed *vs*. diffusion), and the structure, composition, and maturity of the particles under analysis (Apicella et al., 2019; De Iuliis et al., 2011; Michelsen et al., 2007; Migliorini et al., 2020, 2022, 2023a, 2023b; Singh et al., 2019; Török et al.,. 2022; Vander Wal et al., 1998, 1999).

Graphitization of carbon nanoparticles was observed under laser irradiation performed in flame (Vander Wal et al., 1999) as well as *ex-situ* (Apicella et al., 2019; De Iuliis et al., 2011; Vander Wal et al., 1998), as confirmed by TEM analysis. Such effect was ascribed to thermal annealing processes, which are responsible for a change in carbon nanostructure, namely in the order and length of graphitic layers, resulting in an increase in absorption efficiency.

In agreement with these works, laser-induced incandescence measurements performed on laser-heated carbon nanoparticles produced with a mini-CAST (Török et al., 2022) revealed an increase in the LII signal, which was attributed to thermal annealing processes.

Moreover, in the work of Singh et al. (Singh et al., 2019), the nanosecond heating process was proposed as a diagnostic tool to retrieve information on the initial nanostructures parameters of the particles under study and, ultimately, on the related sources. Such an approach can be promising for identifying soot at any pollution monitoring receptor site. In this work, where laser irradiation was performed on different types of soot (e.g. black carbon and flame-ethylene soot) deposited on a TEM grid in a controlled atmosphere, annealing was considered responsible for an increase in the inner structure ordering, dependent on the laser fluence employed for irradiation.

Different observations were reported by Michelsen et al. (Michelsen et al., 2007). In their work, during laser irradiation the formation of new carbon nanoparticles, due to vaporization of carbon fragments and subsequent nucleation, was observed. The physical and chemical processes proposed are in line with the results reported in (Migliorini et al., 2020, 2022a, 2023a, 2023b) which described the effect of laser irradiation on the optical properties of carbon nanoparticles produced in a premixed flame as well as in a quenched diffusion flame (during laser irradiation and after the laser pulse). In particular, in this last case, a significant variation in the spectral behavior of the optical absorption properties was detected in laser-irradiated nanoparticles and it was suggested to be related to a strong fragmentation of the aggregates and/or formation of new particles (Migliorini et al., 2020) as revealed by particle size distribution measurements.

Conversely, the influence of laser irradiation on particles sampled from a premixed flame was found to be related to the particles aging stages (Migliorini, Belmuso, et al., 2023b). While no substantial changes in the optical properties were observed for nascent particles, significant spectral variation of the optical absorption coefficient was detected for mature carbon particles, depending on the fluence of the irradiating laser shot.

The contrasting results reported in the literature highlight that the understanding of the effect of laser irradiation on the structure, morphology, and consequent chemical-physical properties is far from being completely achieved. Moreover, attention has to be paid to the experimental conditions under analysis, particularly to the environment where the laser irradiation process occurs.

The present work aims at deepening this understanding by applying different spectroscopy tools to investigate the effect of laser irradiation on carbon nanoparticle samples with varying degrees of maturity.

Specifically, this work combines in-flow extinction measurements with *ex-situ* FT-IR and Raman spectroscopy analysis. Each technique allows a specific particle characterization in terms of morphological and chemical properties, from the early to the late stage of its formation (Baldelli et al., 2020). In particular, FT-IR spectroscopy enables the analysis of aromatics and aliphatic compounds in nascent particles and the identification of surface functional groups and/or oxidation degrees in mature particles. On the other hand, Raman spectroscopy allows the evaluation of the graphitization level in mature carbon particles. Finally, extinction measurements are employed to investigate the optical absorption properties of the particles under study.

Although many works are reported in the literature on employing these techniques for a complete optical and structural characterization of pristine carbon particles (Ferrari & Basko, 2013; Ferrari and Robertson, 2000, 2001; Sadezky et al., 2005; De Falco et al., 2020; Commodo et al., 2016; Tommasini et al., 2016; Santamaria et al., 2006; Liu et al., 2017; Cain et al., 2010), their application to the analysis of possible particle modification due to laser irradiation represents the novelty of the present work. To our knowledge, FT-IR and Raman spectroscopy analysis have not been yet performed on laser-irradiated nanoparticles, apart from our previous investigation on particles collected from a quenched diffusion flame (Migliorini et al., 2020).

In this work, measurements are carried out on pristine nanoparticles and nanoparticles irradiated with a single laser shot and 10 laser shots. Moreover, to investigate the role of different aging conditions on laser irradiation, we explicitly consider particles sampled from a premixed flame and having different maturity degrees.

2. Experimental

Carbon nanoparticles are produced in a rich premixed ethylene/air flame stabilized on a water-cooled sintered bronze McKenna burner with a stainless-steel plate positioned at 30 mm above the burner. The cold gas velocity is set at 10 cm/s and the carbon to oxygen (C/O) atomic ratio at 0.67, corresponding to an equivalence ratio of 2.0.

The description of the experimental apparatus used for optical extinction measurements was reported in our previous works (Migliorini et al., 2021, 2022b) and is briefly recalled here. Particles and gaseous species are sampled from the center of the flame through a 2 mm diameter orifice of a horizontal stainless-steel sampling probe (10 mm O.D. and 8 mm I.D.) In order to quench chemical reactions, nitrogen is flowing in the sampling probe. The pressure drop in the sampling inlet and the pumping system are

monitored to collect the particles aerosol with a dilution of about 10.

A three-way valve is used to switch between a particle-laden aerosol to a filtered aerosol sample thanks to a glass fiber filter placed in the filtering line. In this way, optical extinction due to carbon nanoparticles can be corrected for the contribution from gaseous species (Migliorini et al., 2021). In this work, the analysis is performed on particles sampled at Z = 8 mm and Z = 14 mm above the burner surface. In fact, particles at these heights represent different aging conditions, in agreement with our previous results (Migliorini et al., 2021, 2022b). For this reason, particles at Z = 8 mm and Z = 14 mm are named nascent and mature, respectively.

After sampling, the aerosol flows through an irradiation unit, consisting of a glass tube where particles are irradiated by a Nd:YAG laser beam (Quantel, Big Sky, CFR 400, 1064 nm, 10 Hz, top-hat beam profile). A portion of the beam selected with an aperture having the same diameter as the glass tube (5 mm i.d.) is properly aligned to irradiate all the particles in the volume (Migliorini, Belmuso, et al., 2023b). To heat the particles with 1 laser shot, a 10 cm tube is used and the pumping rate is set at 1 Nl/min, while for 10 laser shots, particles are flowing in a 66 cm tube and pumped at 0.8 Nl/min. Particles are irradiated with 400 mJ cm^{-2} laser fluence to investigate the impact on their properties. The choice of the laser fluence is explained in the Supplementary Material (SM). Pristine or laser-irradiated particles are then sent to the extinction unit, similar to the one reported in (Migliorini et al. 2022a, 2023, 2023b), consisting of a 450 cm long tube. This is also the pathway of extinction measurements, which is kept constant in all conditions under analysis.

Wavelength-resolved optical extinction measurements are carried out in the 300–834 nm spectral region, using two different light sources: a deuterium lamp (63379 Oriel 30 W) in the 300–450 nm range and a tungsten halogen lamp in the 450–834 nm range. These lamps are selected using a flip mirror. Proper long pass filters are used to avoid second-order contributions. Spectral-resolved signals are collected using a spectrometer, consisting of a Czerny-Turner spectrograph (Shamrock 303i, 150 grooves/mm) coupled with an ICCD camera (iStar 334T, Andor Technology). Each spectrum results from the accumulation of 1000 individual spectra. After the optical extinction-measurement line the particles are collected on a quartz filter (Watmann, ∅ = 47 mm) for subsequent off-line analysis.

For FT-IR measurements, pristine and laser-irradiated particles are removed from the filter, and the powder is positioned on the ATR unit of a Thermo Scientific Nicolet 6700. The spectra are collected with 4 cm^{-1} resolution by accumulating 64 scans.

For Raman Spectroscopy, a HORIBA Jobin Yvon LabRAM Spectrometry is used with a 632 nm wavelength laser source working at a maximum power of 8 mW, and the particles-loaded filter is directly placed under the Raman microscope. The laser wavelength was chosen to reduce the fluorescence background and laser-induced structural modification. Although we are aware that fluorescence emission can provide information on particle structure, we prefer to reduce this background contribution to increase the signal-to-noise ratio. Moreover, to avoid possible structural changes in the particles under analysis, neutral filters are added to reduce the power of the excitation laser beam. For pristine nanoparticles, a 0.6 OD filter is used, while for laser-irradiated nanoparticles, a 1 OD filter is selected. In all conditions, the exposure time is set at 60 s and each measurement is obtained as the average of 3 acquisitions. To compare the Raman spectra of the samples without being affected by background variations (see Fig. 3), we normalize the spectra $R(\nu)$ by the standard normal variate (SNV) transformation, namely: $N(\nu) = [R(\nu) - R_a]/\sigma_R$. R_a denotes the average intensity of the Raman spectrum over the considered spectral range, and σ_R is the standard deviation of the Raman intensity in the same range.

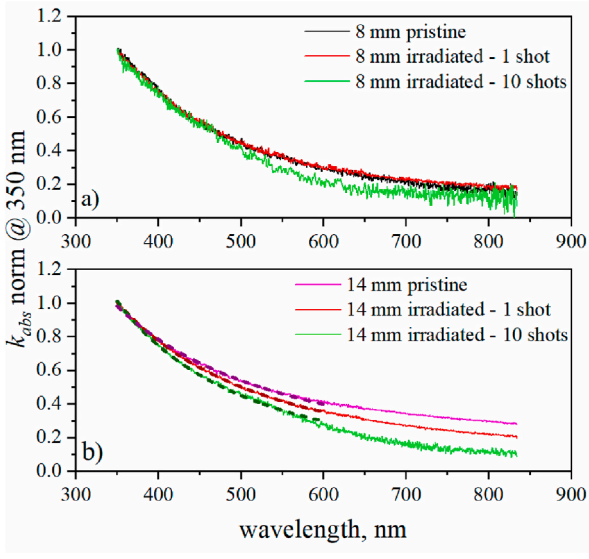

Fig. 1. Absorption coefficient versus wavelength of pristine and laser-irradiated nanoparticles with 1 and 10 laser shots. Spectra are normalized at 350 nm. The dashed lines in (b) indicate the power law fitting in the visible region.

3. Results

According to the Beer–Lambert law, the spectral transmittance $\tau\lambda$, given by the ratio of transmitted to incident light intensity for each wavelength λ, is related to the extinction coefficient *kext,* as $-\ln \tau\lambda = kext\, L$, where L is the optical pathway and *kext* includes the contribution of absorption and scattering coefficients. Considering the scattering negligible (Migliorini, Belmuso, Ciniglia, et al., 2022a), the absorption coefficient can be directly obtained from extinction measurements.

In Fig. 1 the absorption coefficient *kabs* vs. wavelength of pristine and laser-irradiated nanoparticles with single and 10 laser shots is shown.

Both nascent (a) and mature (b) particles spectra are normalized to the value at 350 nm. In fact, during sampling, inlet-probe clogging occurred which made absolute measurements difficult. Normalizing at 350 nm permits to obtain the spectral trend of absorption changes with the height and, in each condition, after laser irradiation. The uncertainty of the absorption coefficient is evaluated to be 8%.

In agreement with our previous results, for nascent particles no relevant changes are obtained after laser irradiation in the spectral trend even with ten laser shots. This is due to the very low absorption coefficient of these particles at 1064 nm. On the contrary, mature particles exhibit significant changes in the spectral trend of the absorption coefficient, which become more pronounced with an increasing number of laser shots.

To underline the differences in these trends, the *kabs* spectra are fitted using the power law function $kabs = c\ \lambda\text{-}\alpha$, where c depends on the particle concentration and α is the dispersion exponent. This parameter provides a measure of the wavelength dependence of the absorption coefficient. In this work, the fitting is performed in the visible spectral region, shown with dashed lines as an example in Fig. 1b. As reported in the literature, since the value of the dispersion exponent is related to the maturity level of the particles under analysis, the following empirical relationship was proposed to retrieve the C/H ratio (Michelsen, 2021)

$$C/H = [(0.39 \pm 0.02)\ \alpha - (0.27 \pm 0.03)]^{-1} \quad (1)$$

According to this relationship, the values of the dispersion coefficient obtained in the conditions under analysis are used to evaluate C/H. The results are reported in Table 1.

Comparing pristine nanoparticles sampled at Z = 8 and 14 mm, a C/H increase is obtained with increasing sampling height, indicating an increase in particle maturity. The values reported here agree with the work by Gurentsov et al. (Gurentsov et al., 2022) despite their measurements are performed in flames with different equivalence ratio.

Considering the effect of laser irradiation, comparing pristine and irradiated nascent nanoparticles similar values in the dispersion exponent are obtained, resulting in similar C/H values. The slight changes detected under ten laser shots irradiation can be considered to lie within the experimental uncertainties. Moreover, it is worth noticing that for pristine nanoparticles sampled at 14 mm the value of the dispersion exponent α increases and correspondingly the C/H ratio decreases under laser irradiation with the number of laser shots. Such behavior suggests that the effect of laser irradiation results in a modification of the structure of the particles towards a less mature level.

We carried out a vibrational spectroscopy characterization with IR and Raman techniques to obtain information about the structure of the collected carbon particles as a function of laser irradiation and collection height.

The results of the FT-IR measurements are displayed in Fig. 2, where selected bands have been labeled to help the reader inspect the spectra. For clarity, we also report in Table 2 the IR peaks observed in our spectra and the corresponding assignments. However, since the absorption properties of nascent particles do not change with laser irradiation, at Z = 8 mm FTIR and Raman analysis is limited only to the case of 1 laser shot.

In the spectral region below 1000 cm^{-1} we observe, especially for the sample collected at Z = 8 mm, several bands typically found in systems with aromatic moieties, and which are assigned to out-of-plane vibrations of aromatic CH bonds (Tommasini et al., 2016). These are the bands observed at 877 cm^{-1} (SOLO, **a**), 835 cm^{-1} (DUO, **b**), 754 cm^{-1} (QUATRO/TRIO, **c**). In contrast, in the sample collected at Z = 14 mm, an evident SOLO signal (873 cm^{-1}, **a**), and the other CH out-of-plane bending markers are less resolved than in the Z = 8 mm case.

For the Z = 8 mm sample, we also observe other out-of-plane ring deformation bands (954 cm^{-1}, **d**; 711 cm^{-1}, **e**; 685 cm^{-1}, **f**; 592 cm^{-1}, **g**; 538 cm^{-1}, **h**) and a shoulder of the QUATRO/TRIO band (736 cm^{-1}) that are assigned to variously substituted non-condensed aromatic moieties (Socrates, 2001). Similar to the case of the CH out-of-plane bending (see Table 2), the latter IR markers are not evident in the pristine sample collected at Z = 14 mm and appear at slightly different positions with respect to the Z = 8 mm sample.

The CH stretching region of the Z = 8 mm sample shows both aliphatic and aromatic CH stretching vibrations, whereas for the Z = 14 mm sample only the aliphatic CH modes (below 3000 cm^{-1}) can be clearly detected, and the aromatic CH stretching are barely

Table 1
Dispersion exponent and C/H values varying the number of laser shots.

# laser shots 400 mJ cm^{-2}	8 mm		14 mm	
	A	C/H	α	C/H
0	2.34	1.56	1.37	3.79
1	2.27	1.63	1.95	2.03
10	2.65	1.31	2.43	1.47

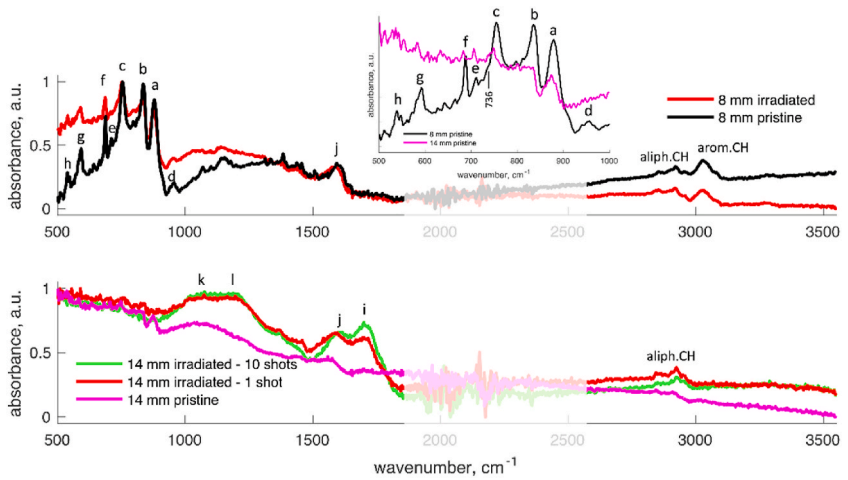

Fig. 2. Normalized ATR spectra of the carbon particles collected at Z = 8,14 mm height above the burner. The spectra of pristine and laser-irradiated samples are compared. The inset compares the IR spectra of the pristine Z = 8 mm and Z = 14 mm samples (for both spectra, the vertical scale has been re-adjusted to help the comparison).

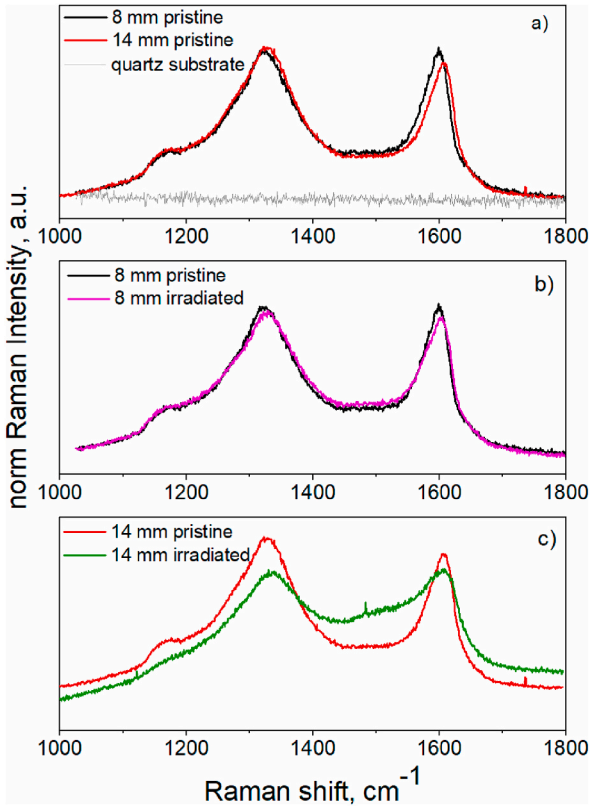

Fig. 3. Raman spectra of the carbon particles collected at Z = 8,14 mm. The spectra of pristine and laser-irradiated samples are compared. The Z = 14 mm sample subjected to 10 laser pulses is not reported due to the temporal variation of the spectrum during the Raman measurement, despite the careful control of laser power.

observable (Fig. 2). Overall, the two samples show a markedly different intensity ratio of the CH stretching and CH out-of-plane bands with respect to the aromatic C=C stretching vibration (1600 cm^{-1}, **j**). This intensity ratio is lower in the Z = 14 mm sample than in the Z = 8 mm sample, which fully agrees with the fact that the C/H ratio of the Z = 8 mm sample is significantly lower than the C/H ratio of the Z = 14 mm sample (Table 2). In other words, there are fewer CH oscillators in the Z = 14 sample than in the Z = 8 mm sample.

Table 2
IR peak observed along with assignment and corresponding reference.

Peak position/[range] (cm^{-1})	Assignment	Ref.
3030	aromatic CH str.	Socrates, 2001
2978-2925-2850	asymm./symm. CH aliphatic str.	Socrates, 2001
1702 (**i**)	carbonyl C=O str.	Socrates, 2001
1600 (**j**)	aromatic C=C str.	Socrates, 2001
1197 (**l**)	epoxy C–O str.; C–O/C–C str.	Hu et al., 2023; Socrates, 2001
1074 (**k**)	alkoxy C–O str. (ethers); C–O/C–C str.	Hu et al., 2023; Socrates, 2001
954 (**d**)	out-of-plane ring deformation	Socrates, 2001
877 (**a**)/[890–910]	SOLO CH out-of-plane bend.	Tommasini et al., 2016
835 (**b**)/[800–860]	DUO CH out-of-plane bend.	Tommasini et al., 2016
754 (**c**)/[730–770]	TRIO/QUATRO CH out-of-plane bend.	Tommasini et al., 2016
736	out-of-plane ring deformation	Socrates, 2001
711 (**e**)	out-of-plane ring deformation	Socrates, 2001
685 (**f**)	out-of-plane ring deformation	Socrates, 2001
592 (**g**)	out-of-plane ring deformation	Socrates, 2001
538 (**h**)	out-of-plane ring deformation	Socrates, 2001

We consider now the effects of laser irradiation. After a single laser shot, the sample collected at Z = 8 mm does not display a strong variation in the IR spectrum, especially concerning the low wavenumber region. The most evident change induced by laser irradiation is the presence of a broad and structured absorption (1000–1500 cm^{-1}) that occurs in the same spectral region as the Z = 14 mm sample. However, for the latter sample, the change is significantly stronger, as it is the rise of a band at 1702 cm^{-1} (**i**), assigned to C=O vibrations. The aromatic C=C stretching vibration at about 1600 cm^{-1} (**j**) is weakly affected by laser irradiation in the Z = 8 mm sample, which is in contrast with the Z = 14 mm sample, which displays a significant increase in intensity and wavenumber shift with laser irradiation.

Furthermore, the Z = 14 mm sample shows with laser irradiation the rise of two broad absorptions at 1074 cm^{-1} (**k**) and 1197 cm^{-1} (**l**) that involve coupled C–C/C–O vibrations.

To summarize the IR results, the Z = 14 mm sample under laser irradiation in exhaust gases is undergoing a significant oxidation, that is not appearing in the Z = 8 mm sample. This is justified by the marked differences in the light absorption properties of the two samples (see Fig. 1 and related discussion).

In Fig. 3 Raman spectra of pristine and laser-irradiated carbon particles collected at Z = 8,14 mm are shown. Unlike IR spectroscopy, which provides global information on the sample molecular structure, Raman spectroscopy of disordered nanostructured carbon species is intrinsically dominated by resonance phenomena (Castiglioni et al., 2004; Ferrari and Robertson, 2000), which means that, out of the wide distribution of structures, we obtain a view of those that resonate with the chosen laser excitation.

For this reason, the Raman spectra of the samples collected at Z = 8 mm and Z = 14 mm appear very similar, since we probe the same kind of molecular structures (same π conjugation), despite the evident difference of the samples as evidenced by IR spectroscopy (Fig. 2). Notably, upon laser irradiation, the Z = 14 mm sample displays a Raman spectrum which deviates significantly from that of the non-irradiated sample, whereas the Z = 8 mm sample does not show major differences in the Raman spectrum upon irradiation. These results parallel those of the IR spectroscopy discussed above and confirm that the Z = 14 mm sample is much more sensitive to laser irradiation than the Z = 8 mm sample. Upon irradiation of the Z = 14 mm sample the D band broadens and shifts to higher wavenumber, suggesting a decrease in π-conjugation, which is consistent with the result of oxidation observed with IR spectroscopy.

The Z = 14 mm sample subjected to 10 laser pulses is not reported due to the temporal variation of the spectrum during the Raman measurement, despite the careful control of laser power.

4. Discussion

By combining the results reported in the previous section concerning spectral absorption coefficient and FT-IR and Raman spectroscopy, it is evident that different effects of laser irradiation are obtained according to the maturity level of the particles under analysis. It is worth noticing that while the absorption coefficient of laser-irradiated nanoparticles produced from a premixed flame has already been reported in our previous works (Migliorini, Belmuso, et al., 2023b), the increase in the number of laser shots and the employment of FT-IR and Raman techniques represent the novelty of this work. Consequently, no data are available in the literature for comparison. The combination of these techniques allows for a clearer description of the processes occurring under laser irradiation.

For nascent particles, no substantial modification occurs, which is essentially due to the low absorption efficiency of these particles in the NIR spectral region (1064 nm). A similar spectral behavior of the absorption coefficient as well as similar features in the Raman spectra are obtained by comparing pristine and laser-irradiated nanoparticles. Regarding the IR analysis, only slight changes in the intensity of the main peaks of the aromatic/aliphatic structures are detected.

However, for mature particles, the effect of laser irradiation is more significant. The changes in the spectral trend of the absorption coefficient are evident. An increase in the dispersion exponent and a resulting decrease in the C/H ratio was evaluated, which is more pronounced by increasing the number of laser shots to 10. Such behavior, in agreement with our previous works, suggests that under laser irradiation complex chemical/physical processes occur leading to a general change of particle properties. This contrasts with the idea that mature particles under laser irradiation undergo annealing processes as suggested in the literature (Apicella et al., 2019;

Török et al., 2022; Vander Wal et al., 1998, 1999). Also in our pioneer work (De Iuliis et al., 2011) we have observed an increase in the incandescence signal irradiating particles sampled from a premixed flame which was attributed to graphitization or annealing processes. However, these measurements were carried out in quite different experimental conditions, and such graphitization was not proved via TEM analysis in soot premixed flame. At this stage, we can not exclude that graphitization may occur as well to some extent but needs to be further investigated.

The findings obtained from extinction measurements are supported by the analysis of IR and Raman spectroscopy.

The Raman spectra of carbonaceous materials are commonly analyzed with a fit of five different bands, namely D4, D1′, D1, D3 and G, following the approach proposed in the literature (Sadezky et al., 2005; Russo et al., 2015). In particular, the combination of a Gaussian curve for the D3 band, Lorentzian curve for the D4, D1, and D1' bands, and Breit-Wigner-Fano (BWF) for G was found to generate with floating peak locations the lowest χ^2 sums and the highest coefficients of determination (R^2). As for the G peak, BWF fitting function permits to better describe the asymmetric behavior of this band, resulting from the presence of G and D2 contribution (Russo et al., 2015).

Fig. 4 shows the Raman spectra of pristine (a) and irradiated (b) particles sampled at 14 mm and the corresponding fitting curves.

To evaluate the contribution of each band to the total spectrum (Sadezky et al., 2005), the ratios of the intensities of the individual D bands to the intensity of the G band are reported in Table 3 together with the bandwidth (FWHM) of the D1 and G peak. According to the literature (Casiraghi et al., 2005; Russo et al., 2015), FWHM(D1) and FWHM(G) values are related to structural disorder, namely the aromatic cluster distribution and the layer distortion of aromatic clusters, respectively. Moreover, the effect on the area of D1 peak with respect to the one of G peak (A(D1)/A(G)) is also investigated and reported in the same Table 3.

By comparing the results from pristine and laser-irradiated carbon nanoparticles, a complex picture of what happens under laser irradiation can be drawn. The peak intensity ratio of I(D1)/I(G), which gives information on the order degree of amorphous carbon exhibits a slight increase for the particles after irradiation. On the contrary, similar values are obtained for A(D1)/A(G) of pristine and irradiated particles. The different trend obtained (decrease in intensity ratio vs almost unchanged values for the corresponding area ratio) is due to a different increase under irradiation in FWHM(G) and FWHM(D1): the bandwidth of D1 increases of 15%, whilst an enhancement of 30% is detected for G bandwidth. Such behavior can be justified considering the amorphous character of soot particles. Therefore, in our measurements, laser irradiation seems to enable even higher degree of disorder within the particles.

As for the other Raman peaks analyzed, while no substantial differences in I(D1')/I(G) and I(D4)/I(G) are detected with laser irradiation, the I(D3)/I(G) intensity ratio, attributed to amorphous carbon, exhibits a significant increase comparing pristine and irradiated nanoparticles, confirming the overall trend previously described. Moreover, the increase in this intensity ratio can be related to a decrease in EC/TC (elemental-to-total carbon) as reported in the literature (Ivleva et al., 2007).

Therefore, from Raman spectra, we can say that laser irradiation promotes the increase in amorphous carbon content due to molecular/organic compounds and/or disorder due to vaporization/and growing of new particles. Considering FT-IR analysis, oxidation processes occur upon laser irradiation, as confirmed by the rise of the C=O stretching band (1702 cm-1, i), and broad C–O/C–C stretching bands (1074 cm-1, k; 1197 cm-1, l) that are also observed in graphene oxide samples (Hu et al., 2023). We observe that, compared to the typical IR spectra of graphene oxide samples, the IR spectrum of the irradiated Z = 14 mm sample shows much broader bands, which suggests a much wider structural disorder and variety of chemical structures, in line with the Raman spectroscopy analysis.

These results are in agreement with the work by Cuong Le et al. (Cuong Le et al., 2024), where the effect of laser irradiation during Raman measurements has been investigated in different oxidation conditions and resulting in structural modification due to oxidation processes. However, since in their work a decrease in D3 peak intensity is detected, they attributed the structural modification to defects instead of amorphization.

To conclude, oxidation processes and the presence of structures spectroscopically correlated with graphene oxide proves that under laser irradiation the carbon particles exhibit a significant modification, probably promoted by the specific ambient condition where laser irradiation is performed (exhaust gases, in the present case). The investigation of laser irradiation in different ambient conditions could open other reaction pathways, which require more work to be done in this prospective.

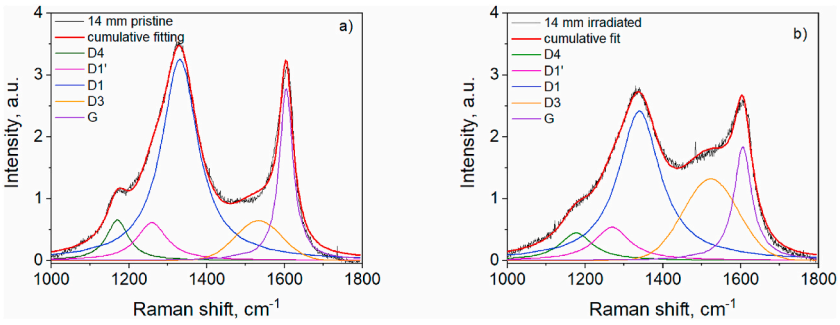

Fig. 4. Five-band curve fitting of carbon particles Raman spectra of pristine and laser-irradiated particles sampled at 14 mm. The D1, D4, and D1′ bands are fitted with a Lorentzian curve, the D3 band is fitted with a Gaussian curve, and G band with BWF function.

Table 3
D1 and G peak bandwidths, intensity ratio of D1, D1', D3 and D4 with respect to G peak, and the ratio of D1 and G peak area for pristine and laser-irradiated particles at 14 mm.

	14 mm pristine	14 mm irradiated
FWHM(D1), cm^{-1}	113	130
FWHM(G),cm^{-1}	42	55
I(D1)/I(G)	1.17	1.32
A(D1)/A(G)	3.02	3
I(D1')/I(G)	0.22	0.29
I(D3)/I(G)	0.23	0.72
I(D4)/I(G)	0.23	0.24

5. Conclusions

In this work, the different response of combustion-generated carbon nanoparticles in the application of laser diagnostic tools is investigated, depending on the variety of initial optical and physicochemical properties of the particles under analysis. To this purpose, by coupling absorption measurements with FT-IR and Raman spectroscopy, information on optical, chemical and structural properties of pristine and laser-irradiated particles in different aging stages are obtained.

It was observed that while nascent particles show no substantial changes under laser irradiation, significant effects are revealed for mature particles with these effects becoming more pronounced as the number of laser shots increases. In particular, the changes in the chemical structure witnessed by the changes in the vibrational spectra, indicate a complex modification of the particles under analysis, with an increase in the crystallite size detected from Raman spectroscopy as well as an increase in the amorphous carbon amount due to vaporization and formation of new particles under laser irradiation.

Moreover, FT-IR spectra indicating the presence of oxygenated groups similar to those observed in graphene oxide spectra suggests that under laser irradiation soot particles exhibit an increasing tendency to undergo chemical reactions. These reactions are promoted by the high temperature (almost 4000 K) reached by the particles in the surrounding combustion exhaust gases. Additionally, the specific ambient conditions where laser irradiation is performed (exhaust gases, in this case) may play a role in the formation of oxidized species.

To conclude, significant physical and chemical processes can be responsible for the effects observed on the carbon particles under laser irradiation, although at this stage it is difficult to evaluate and separate the two contributions. However, the modification of particle optical and physicochemical properties cannot be neglected for a correct implementation of the optical diagnostics for monitoring purposes. It is extremely important to consider the initial absorption properties of the particles under analysis as well as the effect of the laser shot on these properties, which can be widely different in each specific condition.

CRediT authorship contribution statement

Francesca Migliorini: Writing – review & editing, Writing – original draft, Investigation, Formal analysis, Conceptualization. **Roberto Dondé:** Writing – review & editing, Writing – original draft, Investigation, Conceptualization. **Andrea Lucotti:** Writing – review & editing, Formal analysis. **Mauro Fasoli:** Investigation. **Matteo Tommasini:** Writing – review & editing, Formal analysis. **Silvana De Iuliis:** Writing – review & editing, Writing – original draft, Methodology, Formal analysis, Conceptualization.

Declaration of competing interest

The authors declare that they have no known competing financial interests or personal relationships that could have appeared to influence the work reported in this paper.

Data availability

Data will be made available on request.

Acknowledgements

The authors would like to acknowledge the financial support from the PRIN project 2017PJ5XXX: ''Modeling and Analysis of carbon nanoparticles for innovative applications Generated dIrectly and Collected During combuSTion (MAGIC DUST)''.

Appendix A. Supplementary data

Supplementary data to this article can be found online at https://doi.org/10.1016/j.jaerosci.2024.106440.

References

Apicella, B., Pré, P., Rouzaud, J. N., Abrahamson, J., Vander Wal, R. L., Ciajolo, A., Tregrossi, A., & Russo, C. (2019). Laser-induced structural modifications of differently aged soot investigated by HRTEM. *Combustion and Flame, 204*, 13–22. https://doi.org/10.1016/j.combustflame.2019.02.026

Baldelli, A., Trivanovic, U., Sipkens, T. A., & Rogak, S. N. (2020). On determining soot maturity: A review of the role of microscopy- and spectroscopy-based techniques. *Chemosphere, 22*, Article 126532. https://doi.org/10.1016/j.chemosphere.2020.126532

Cain, J. P., Gassman, P. L., Wang, H., & Laskin, A. (2010). Micro-FTIR study of soot chemical composition-evidence of aliphatic hydrocarbons on nascent soot surface. *PCCP: Physical Chemistry Chemical Physics, 12*, 5206–5218. https://doi.org/10.1039/B924344E

Casiraghi, C., Ferrari, A. C., & Robertson, J. (2005). Raman spectroscopy of hydrogenated amorphous carbons. *Physical Review B: Condensed Matter, 72*, Article 085401. https://doi.org/10.1103/PhysRevB.72.085401

Castiglioni, C., Tommasini, M., & Zerbi, G. (2004). Raman spectroscopy of polyconjugated molecules and materials: Confinement effect in one and two dimensions. *Philosophical Transactions of the Royal Society of London - A, 362*, 425–2459. https://doi.org/10.1098/rsta.2004.1448

Commodo, M., De Falco, G., Larciprete, R., D'Anna, A., & Minutolo, P. (2016). On the hydrophilic/hydrophobic character of carbonaceous nanoparticles formed in laminar premixed flames. *Experimental Thermal and Fluid Science, 73*, 56–63. https://doi.org/10.1016/j.expthermflusci.2015.09.005

Cuong Le, K., Bergqvist, S., Henriksson, J., & Bengtsson, P. E. (2024). Observation of structural changes during oxidation of black and brown soot using Raman Spectroscopy. *Journal of Carbon Research, 10*, 38. https://doi.org/10.3390/c10020038

De Falco, G., Picca, F., Commodo, M., & Minutolo, P. (2020). Probing soot structure and electronic properties by optical spectroscopy. *Fuel, 259*, Article 116244. https://doi.org/10.1016/j.fuel.2019.116244

De Iuliis, S., Cignoli, F., Maffi, S., & Zizak, G. (2011). Influence of the cumulative effects of multiple laser pulses on laser-induced incandescence signals from soot. *Applied Physics B, 104*, 321–330. https://doi.org/10.1007/s00340-011-4535-y

Ferrari, A. C., & Basko, D. M. (2013). Raman spectroscopy as a versatile tool for studying the properties of graphene. *Nature Nanotechnology, 8*, 235. https://doi.org/10.1038/nnano.2013.46

Ferrari, A. C., & Robertson, J. (2000). Interpretation of Raman spectra of disordered and amorphous carbon. *Physical Review B, 61*(20), Article 14095. https://doi.org/10.1103/PhysRevB.61.14095

Ferrari, A. C., & Robertson, J. (2001). Resonant Raman spectroscopy of disordered, amorphous, and diamonlike carbon. *Physical Review B, 64*, Article 075414. https://doi.org/10.1103/PhysRevB.64.075414

Gurentsov, E. V., Eremin, A. V., Kolotushkin, R. N., & Khodyko, E. S. (2022). Correlation of changes in optical properties of soot particles synthesized in a premixed flame with increasing mean particle size. *B. Lebedev Phys. Inst., 49*(12), 422–428. https://doi.org/10.3103/S1068335622120028

Hu, K., Brambilla, L., Sartori, P., Moscheni, C., Perrotta, C., Zema, L., Bertarelli, C., & Castiglioni, C. (2023). Development of tailored graphene nanoparticles: Preparation, sorting and structure assessment by complementary techniques. *Molecules, 28*, 565. https://doi.org/10.3390/molecules28020565

Ivleva, N. P., McKeon, U., Niessner, R., & Poschl, U. (2007). Raman microspectroscopic analysis of size-resolved atmospheric aerosol particle samples collected with an ELPI: Soot, humic-like substances, and inorganic compounds. *Aerosol Science & Technology, 41*(7), 655–671. https://doi.org/10.1080/02786820701376391

Liu, Y., Fan, C., Li, N., & Wang, X. (2017). Surface functional groups and graphitization degree of soot in the sooting history of methane premixed flame. *SAE Technical Paper 2017-01-1003*. https://doi.org/10.4271/2017-01-1003

Michelsen, H. A. (2017). Probing soot formation, chemical and physicalevolution, and oxidation: Areview of *in situ* diagnostic techniques and need. *Proceedings of the Combustion Institute, 36*, 717–735. https://doi.org/10.1016/j.proci.2016.08.027

Michelsen, H. A. (2021). Effects of maturity and temperature on soot density and specific heat. *Proceedings of the Combustion Institute, 38*, 1197–1205. https://doi.org/10.1016/j.proci.2020.06.383

Michelsen, H. A., Colket, M. B., Bengtsson, P. E., D'Anna, A., Desgroux, P., Haynes, B. S., Miller, J. H., Nathan, G. J., Pitsch, H., & Wang, H. (2020). A Review of terminology used to describe soot formation and evolution under combustion and pyrolytic conditions. *ACS Nano, 14*, 12470–12490. https://doi.org/10.1021/acsnano.0c06226

Michelsen, H. A., Tivanski, A. V., Gilles, M. K., van Poppel, L. H., Dansson, M. A., & Buseck, P. R. (2007). Particle formation from pulsed laser irradiation of soot aggregates studied with a scanning mobility particle sizer, a transmission electron microscope, and a scanning transmission x–ray microscope. *Applied Optics, 46*(6), 959–977. https://doi.org/10.1364/AO.46.000959

Migliorini, F., Belmuso, S., Ciniglia, D., Dondè, R., & De Iuliis, S. (2022a). A double pulse LII experiment on carbon nanoparticles: Insight into optical properties. *PCCP: Physical Chemistry Chemical Physics, 24*, Article 19837. https://doi.org/10.1039/D2CP02639B

Migliorini, F., Belmuso, S., Ciniglia, D., Dondé, R., & De Iuliis, S. (2023b). Laser irradiation of different-aging carbon nanoparticles: Study of the effect on optical properties. *Applied Physics B: Lasers and Optics, 129*, 133. https://doi.org/10.1007/s00340-023-08078-9

Migliorini, F., Belmuso, S., Dondé, R., & De Iuliis, S. (2021). In-flow optical characterization of flame-generated carbon nanoparticles sampled from a premixed flame. *PCCP: Physical Chemistry Chemical Physics, 23*, Article 15702. https://doi.org/10.1039/D1CP01267C

Migliorini, F., Belmuso, S., Dondè, R., De Iuliis, S., & Altman, I. (2022b). To optical properties of carbon nanoparticles: A need in comprehending urbach energy. *Carbon Trends, 8*, Article 100184. https://doi.org/10.1016/j.cartre.2022.100184

Migliorini, F., De Iuliis, S., Dondè, R., Commodo, M., Minutolo, P., & D'Anna, A. (2020). Nanosecond laser irradiation of soot particles: Insights on structure and optical properties. *Experimental Thermal and Fluid Science, 114*, Article 110064. https://doi.org/10.1016/j.expthermflusci.2020.110064

Migliorini, F., Dondè, R., & De Iuliis, S. (2023a). Spectral Investigation of soot absorption properties during laser-induced incandescence measurements. *Applied Physics B: Lasers and Optics, 123*, 90. https://doi.org/10.1007/s00340-023-08036-5

Russo, C., & Ciajolo, A. (2015). Effect of the flame environment on soot nanostructure inferred by Raman spectroscopy at different excitation wavelengths. *Combustion and Flame, 162*, 2431–2441. https://doi.org/10.1016/j.combustflame.2015.02.011

Sadezky, A., Muckenhuber, H., Grothe, H., Niesser, R., & Pöschl, U. (2005). Raman microspectroscopy of soot and related carbonaceous materials: Spectral analysis and structural information. *Carbon, 43*, 1731–1742. https://doi.org/10.1016/j.carbon.2005.02.018

Santamaria, A., Mondragon, F., Molina, A., Marsh, N. D., Eddings, E. G., & Sarofim, A. F. (2006). FT-IR and HNMR characterization of the products of an ethylene inverse diffusion flame. *Combustion and Flame, 146*, 52–62. https://doi.org/10.1016/j.combustflame.2006.04.008

Singh, M., Gaddam, C. K., Abrahason, J. P., & Vander Wal, R. L. (2019). Soot differentiation by laser derivatization. *Aerosol Science & Technology, 53*(2), 207–229. https://doi.org/10.1080/02786826.2018.1554243

Socrates, G. (2001). *Infrared and Raman characteristic group frequencies: Tables and charts* (3rd ed.). Chichester: John Wiley and Sons, Ltd.

Tommasini, M., Lucotti, A., Alfè, M., Ciajolo, A., & Zerbi, G. (2016). Fingerprints of polycyclic aromatic hydrocarbons (PAHs) in infrared absorption spectroscopy. *Spectrochimica Acta, Part A, 152*, 134–148. https://doi.org/10.1016/j.saa.2015.07.070

Török, S., Mannazhi, M., Bergqvist, S., Cuong Le, K., & Bengtsson, P.-E. (2022). Influence of rapid laser heating on differently matured soot with double-pulse laser-induced incandescence. *Aerosol Science & Technology, 56*(6), 488. https://doi.org/10.1080/02786826.2022.2046689

Vander Wal, R. L., & Choi, M. Y. (1999). Pulsed laser heating of soot: Morphological changes. *Carbon, 37*(2), 231–239. https://doi.org/10.1016/S0008-6223(98)00169-9

Vander Wal, R. L., Ticich, T. M., & Stephens, A. B. (1998). Optical and microscopy investigations of soot structure alterations by laser-induced incandescence. *Applied Physics B, 67*(1), 115–123. https://doi.org/10.1007/s003400050483